One-equation model to assess population balance kernels in turbulent bubbly flows

Frederic Augier, Eleonora Gilli, Pedro Maximiano Raimundo

One-equation model to assess population balance kernels in turbulent bubbly flows

Frederic Augier, Eleonora Gilli, Pedro Maximiano Raimundo

IFP Energies nouvelles, Rond-point de l'échangeur de Solaize, BP 3, 69360 Solaize, France

Highlights:

- Development of a simplified population balance model to predict Sauter diameter.
- Identification of the best kernels over 60 possible combinations.
- Flows in a bubble column and a stirred tank are considered, leading to two different sets of PBM kernels.
- Kernels suitable to both flows are also reported.

Keywords: Multiphase reactors, Population Balance, Model, Bubble column, Stirred reactor.

Abstract

A simplified population balance model has been developed to predict the Sauter mean diameter, and to optimize any breakage and coalescence kernel. Firstly, the shortcut model is detailed, and the simplifying assumptions are argued. Then the model is applied in a comparison of 60 combinations of a selection of classical breakage, collision frequency and coalescence efficiency kernels. The models are fitted and then compared with an experimental dataset measured in two different technologies of interest for biotechnology: bubble columns (Gemello et al., 2018), and stirred tanks (Cappello et al., 2020). The best kernels are identified for each flow configuration separately, and some kernels are identified as giving acceptable predictions simultaneously of both flows (average error on bubble size< 20%).

Introduction

The use of CFD to simulate two-fluid flows still faces the difficulty to predict representative bubble or droplet size distributions. Currently, the simulation of industrial reactors can only be considered using an Eulerian description of both phases, wherein the dispersed phase is described by its volume-averaged phase fraction. However, size distribution properties – beginning with the Sauter mean diameter d_{32} – are required to correctly predict the mean flow, as they condition interfacial forces, turbulence properties and all transport phenomena between phases. To overcome this issue, population balance models (PBM) are essential tools as they offer the possibility to predict size distributions and make CFD models fully predictive. But in practice, the use of PBM leads to different questions linked to a) the choice of the breakage and coalescence kernels, among dozens of possible choices (Liao & Lucas 2009, 2010) ; b) the quality of the calculation of the local gas fraction (α) and the dissipation rate (ε), which conditions the results of PBM models ; and c) the difficulty to validate PBM as experimental data under industrial relevant conditions are scarce. As a consequence, it still does not exists a real state-of-the-art concerning PBM selection regarding its different applications. CFD users try to elaborate their own "best practices" guides including CFD closure laws, PBM and associated parameters fit. However, as validation steps require 3D multiphase simulations, the possibility to compare physical kernels is narrow and PBM models can hardly be extensively compared on a rational and objective way.

The present study relates an attempt to develop a simple shortcut method able to discriminate the adequacy of kernel combinations in different kinds of bubbly flows. The theoretical background, the main assumptions and the numerical method are presented in the next section. Obviously the objective of the following simplified calculations is not to replace fully predictive CFD simulations coupled with PBM, but rather to help final users to make a choice before

validation or final parameter fit with CFD. Some proposed assumptions are questionable and may impact the results of PBM. For this reason, only qualitative results and guiding ideas are expected from the proposed method. The governing principles of the shortcut method are:

- Volume averaged gas holdup and dissipation rate are considered to screen PBM kernels.
- The Quadrature Method of Moments (QMOM) formalism is followed, but only one moment (the 2nd) is solved.
- Only the Sauter mean bubble size is calculated and used in the shortcut for breakage and coalescence calculations.
- The final "stable" bubble size is computed. The bubble residence time is assumed to be higher than the transient time required to achieve the bubble stable size under a given set of hydrodynamic conditions.

After being detailed, the method is applied on two different bubbly flows: a bubble column and an aerated stirred tank. Results are compared with available experimental data of Gemello et al. (2018) and Cappello et al. (2020), in regard with the associated experimental uncertainty. Best kernel combinations, among a consequent but non-exhaustive panel of possibilities, are pointed out for each investigated case. Finally, the possibility to validate a common "robust" kernel for both cases is discussed.

Method

QMOM framework

The Quadrature Method of Moments is a powerful method that allows to calculate accurately a given number of moments of the Bubble Size Distribution (BSD) (Marchisio et al., 2003 ; Petitti et al., 2010 ; Buffo et al. 2013). The BSD is not discretized in classes of bubble sizes – which is very heavy in term of CPU time, but only the n-th first moments of the BSD are transported.

Based on the knowledge of the first $2N_q$ moments of the BSD, different algorithms lead to the calculation, at each time, of the N_q abscissa of the quadrature approximation:

$$m_k \approx \sum_{i=1}^{N_q} w_i L_i^k \quad (1)$$

where m_k is k^{th} moment of the BSD, L_i are the N_q abscissa of the quadrature approximation (McGraw, 1997). w_i are the weights of the quadrature approximation. A good compromise between accuracy and CPU-time consumption consists to use the 6^{th} first moments of the BSD (k=0 to 5), and thus to approximate the BSD by 3 nodes (L_1, L_2, L_3) with associated weights. The dynamic evolution of moments is governed by the following balance:

$$\frac{dm_k}{dt} = \frac{1}{2}\sum_{i=1}^{3} w_i \sum_{j=1}^{3} w_j h_0(L_i, L_j)\lambda(L_i, L_j)\left[\left({L_i}^3 + {L_j}^3\right)^{\frac{k}{3}} - L_i^k - L_j^k\right] + \sum_{i=1}^{3} w_i g(L_i)\left(\bar{b}_i^k - L_i^k\right) \quad (2)$$

where $h_0(L_i, L_j)$ denotes the collision frequency between 2 bubble nodes, and $\lambda(L_i, L_j)$ its associated coalescence efficiency. $g(L_i)$ is the breakage kernel (breakage frequency model). $\bar{b}_i^k$ is the k^{th} moment of the daughter size distribution β. $\bar{b}_i^k$ impacts the production rate of m_k associated to production of daughter bubbles during the breakage of a bubble of diameter L_i. $\bar{b}_i^k$ writes as follows:

$$\bar{b}_i^k = \int_0^{L_i} \beta(L, L_i) L^k dL \quad (3)$$

$\beta(L, L_i)$ is the daughter bubbles size distribution for a bubble subject to breakage of size L_i. One can identify in Eq.2 death and birth terms associated with breakage and coalescence events. Table 1 reports 5 classical breakage models, 4 collision frequency models and 3 coalescence efficiency models that are considered in the present work. Details of the models are available in literature (Liao & Lucas, 2009,2010).

Table 1: population balance models used in the study. B: breakage, CF: collision frequency, CE: coalescence efficiency

Authors	Model	Constants	Type	Name
Coulaloglou & Tavlarides (1977)	$c_1 L^{-2/3} \frac{\varepsilon^{1/3}}{1+\alpha} \exp\left[-\frac{c_2 \sigma (1+\alpha)^2}{\rho_g \varepsilon^{2/3} L^{5/3}}\right]$	c_1=0.00481 c_2=0.08	B	bCT
Prince & Blanch (1990) Lasheras (2002)	$c_1 L^{-2/3} \frac{\varepsilon^{1/3}}{1+\alpha} \exp\left[-\frac{c_2 \sigma (1+\alpha)^2}{\rho_l \varepsilon^{2/3} L^{5/3}}\right]$	c_1=0.00481 c_2=0.08	B	bPB
Laakkonen (2006)	$c_3 \varepsilon^{1/3} \mathrm{erfc}\left(\sqrt{c_4 \frac{\sigma}{\rho_l \varepsilon^{2/3} L^{5/3}} + c_5 \frac{\mu_l}{\sqrt{\rho_g \rho_l} \varepsilon^{1/3} L^{4/3}}}\right)$	c_3=4, c_4=0.04 c_5=0.01	B	bLa
Lehr(1999)	$0.5 \frac{L^{5/3} \varepsilon^{19/15} \rho_l^{7/5}}{\sigma^{7/5}} \exp\left(-\frac{\sqrt{2}\sigma^{9/5}}{L^3 \rho_l^{9/5} \varepsilon^{6/5}}\right)$		B	bLe
Carrica & Clausse (1993)	$g^* \frac{(L-L_{cr})^m}{(L-L_{cr})^m + L_{cr}^m}$	L_{cr}=0.027m g^* =100s^{-1}, m=6	B	bCC
Prince & Blanch (1990)	$C'_1 (L_1+L_2)^2 \varepsilon^{1/3} \sqrt{L_1^{2/3}+L_2^{2/3}}$	C'_1=0.76 in this work	CF	cfPB
Wang (2005)	$C'_2 \frac{\alpha_{max}}{\alpha_{max}-\alpha} \left[1-\exp\left(-C \frac{\alpha_{max}^{1/3} \alpha^{1/3}}{\alpha_{max}^{1/3}-\alpha^{1/3}}\right)\right] \left(L_i+L_j\right)^2 \varepsilon^{1/3} \sqrt{L_i^{2/3}+L_j^{2/}}$	C'_2=0.17 in this work α_{max}=0.8 C=3	CF	cfW
Lehr (1999)	$C'_2 \exp\left[-\left(\frac{\alpha_{max}^{1/3}}{\alpha^{1/3}}-1\right)^2\right] \left(L_i+L_j\right)^2 \varepsilon^{1/3} \sqrt{L_i^{2/3}+L_j^{2/3}}$	C'_2=0.17 in this work α_{max}=0.6	CF	cfLe
Chesters (1991)	$C(L_1+L_2)^3 \sqrt{\frac{\varepsilon}{\nu}}$	$C=\frac{0.618}{8}$	CF	cfC
Coulaloglou & Tavlarides (1977)	$\exp\left[-C''_1 \frac{\mu_l \rho_l \varepsilon}{\sigma^2 (1+\alpha_g)^3} \left(\frac{L_1 L_2}{L_1+L_2}\right)^4\right]$	C''_1=6.10^{-9}	CE	ceCT
Chesters (1991)	$\exp\left(-\sqrt{\frac{\rho_l \varepsilon^{2/3} L^{5/3}}{4\sigma}}\right)$		CE	ceC
Lehr (1999)	$\min\left(\frac{u_{crit}}{\sqrt{2}\varepsilon^{1/3}\sqrt{L_i^{2/3}+L_j^{2/3}}}, 1\right)$	u_{crit}=0.08m/s	CE	ceLe

A selection of kernels based on the adequacy of their initial conditions of use is commendable but too restrictive in practice. PBM kernels are generally developed in a specific scope, within a given range of physical properties. But they are later applied on miscellaneous systems and operating conditions, sometimes far-off their initial range of validation. In the present study, it was preferred to not presuppose the adequacy (or inadequacy) of kernels, as is often the case in industry, with very partial knowledge on physical or interface properties.

Model simplifications

QMOM models are a very good alternative to the method of classes, especially if the full BSD is not especially required. This is the case when d_{32} is sufficient to describe hydrodynamics and transfer mechanisms. As $d_{32}=m_3/m_2$, and as m_3 is directly linked to the volume averaged gas fraction ($m_3 = 6\alpha/\pi$). If α is calculated by a two-fluid model or known by other means, the only missing moment to estimate d_{32} is m_2. Furthermore, in practice BSD is not measurable, especially when the gas volume fraction α is higher than 1-2%. The two accessible properties of BSD are α and d_{32}. Recent advances allow to measure accurately d_{32} in turbulent bubbly flows with a novel optical probe technique, even at high gas fraction (Raimundo et al., 2016), but no information is given about other moments as neither BSD nor chord size distributions are measured.

Besides, Lane et al. (2005), suggest to solve one equation to estimate a bubble density number. The solved equation is based on breakage and coalescence rates involving only one node quadrature. A similar idea is followed in the present work, and only d_{32} is considered as a node of the BSD. So $L_1 = L = d_{32}$, and L_2 and L_3 does not exist anymore ($w_2=w_3=0$). Besides w_1 is directly linked to the gas volume fraction: $w_1=w = 6\alpha/(\pi L^3)$. As only one node is considered, only one moment is computed, thus only the m_2 equation is solved in the present work, as m_3 is deduced from α. Other moments are not considered.

Eq.2 takes the reduced form:

$$\frac{dm_2}{dt} = \frac{6\alpha}{\pi L}\left[\frac{3\alpha}{\pi L^3}h(L,L)\left(2^{\frac{2}{3}}-2\right) + g(L)(b^2/L^2-1)\right] \quad (4)$$

Another strong assumption consists to solve Eq.4 at steady state ($dm_2/dt = 0$). The assumptions listed above state that under given flow conditions, the PBM reaches quickly a stable d_{32} which is representative of the volume average bubble size. This assumption is in agreement with recent observations in bubble columns (Gemello et al., 2018), where a stable bubble size was observed at a distance of 25cm from the gas distributor. The same assumption is

more discussable in the case of stirred tanks, but QMOM calculations lead to stable bubble sizes after a few seconds, and this time is considered low compared to the residence time of bubbles at any scale. Cappello et al. (2020) found very similar average bubble sizes in stirred tanks of height 0.3m and 0.6m, at equal power input and V_{sg}, showing that the residence time is sufficient at the smaller scale to reach a stable Sauter mean diameter.

The last assumption consists to consider volume averaged values of α and ε to calculate the mean bubble diameter. Concerning bubble columns, this assumption has already been validated during the study of Gemello (2018), who found close results comparing a 0D approach with QMOM to a fully coupled CFD/QMOM modelling. Concerning stirred tanks the assumption is once again more questionable as heterogeneities of dissipation rate are potentially more pronounced. However, it is known for decades that mass transfer inside stirred tanks does not depend on the size of the vessels, neither on the impeller geometry, but it rather depends on average turbulent dissipation rate and superficial gas velocity V_{sg} (Garcia Ochoa & Gomez, 2009 ; Gabelle et al., 2011). As the bubble size is the major physical length that governs mass transfer, it strengthens the idea that the average bubble size is governed by average dissipation rate and gas holdup. Finally, one may keep in mind that the model of Coulaloglou & Tavlarides was initially developed in 0D, which did not prevent it from becoming a reference for PBM. Passing from 0D to CFD may require a parameter tuning in some cases to overcome the non-linear effect of the dissipation rate on the Sauter mean diameter.

Starting from Eq.4, considering the steady state and homogeneous hydrodynamics conditions lead to the following expression:

$$L^3 = \frac{3\alpha h_0(L,L)\lambda(L,L)\left(2^{\frac{2}{3}}-2\right)}{\pi g(L)(1-\bar{b}^2/L^2)} \tag{5}$$

where $\bar{b}^2$ is the contribution of daughter bubbles to the production of m_2. It is strongly linked to the daughter size distribution as smaller bubbles induce more surface per unit of volume of gas. Considering the case of binary breakup, several cases are considered. In Table 2, $\bar{b}_i^k$ expressions are established for different β shapes: asymetric law of Laakkonen (2006), parabolic bell, inverse bell (U shape), and flat shape. Associated analytical expressions of $\bar{b}_i^k$ are all proportional to L_i^k. As a consequence $\bar{b}_i^2/L_i^2$ ratios only depend on the considered β shape, and $\left(1-\bar{b}^2/L^2\right)$ term in Eq.5 is a constant. Therefore, for a given set of PBM kernels, changing the β function and one parameter in one of the models will lead to exactly the same results on d_{32}. For example if we use the β law of Laakkonen and the collision model of Wang with the constant C_2'=0.17, results are exactly the same than with the β bell shape and C_2'=0.24.

Table 2: Considered Models of binary daughter size distribution

Daughter Size Distribution	$\beta(L,L_i)$	$\bar{b}_i^k$	$\bar{b}_i^2/L_i^2$
Laakkonen (2006)	$180\left(\frac{L^2}{L_i^3}\right)\left(\frac{L^3}{L_i^3}\right)\left(1-\frac{L^3}{L_i^3}\right)$	$\frac{3240L_i^k}{(k+9)(k+12)(k+15)}$	≈1.238
Bell	$\frac{70}{3L_i}\left(\frac{L^3}{L_i^3}\right)\left(1-\frac{L^3}{L_i^3}\right)$	$\frac{70L_i^k}{(k+4)(k+7)}$	≈1.333
Inverse bell	$\frac{560}{11L_i}\left(\frac{1}{4}-\left(\frac{L^3}{L_i^3}\right)\left(1-\frac{L^3}{L_i^3}\right)\right)$	$\frac{140(k^2-k+16)L_i^k}{11(k+1)(k+4)(k+7)}$	≈1.296
Flat profile	$\frac{4}{L_i}$	$\frac{4L_i^k}{(k+1)}$	≈1.414

For one condition of gas volume fraction and dissipation rate, Eq.5 has only one unknown variable (L) that can be easily solved with an iterative method. In order to fit a PBM kernel to experimental data, a possibility consists to modify the first constant in one of the PB models. For example the first constant of the collision frequency model could be adjusted. But instead of changing a constant, a correction factor *cf* is introduced in the numerator of Eq.5. The *cf* parameter can be adjusted to minimize the average error between a set of experimental data and the related bubble size predictions. For instance, to fit the predicted bubble size at a known value L, under given conditions (α, ε), the following explicit expression can be used:

$$cf = \frac{L^3 \pi g(L)\left(1-\bar{b}^2/L^2\right)}{3\alpha h_0(L,L)\cdot\lambda(L,L)\left(2^{\frac{2}{3}}-2\right)} \quad (6)$$

Alternatively, *cf* can be estimated to minimize the average error of prediction over a dataset of experimental measurements, as reported in the Results section. The introduction of the *cf* coefficient amounts to modify only one of the first constants of any model reported in Table 1, as the C_1 constant of the breakage model of Coulaloglou and Tavlarides for instance. But the fit of internal constants as C_2 in the same model is not considered in the frame of the present study.

Experimental data

The experimental data of Gemello et al. (2018), dedicated to bubble columns, are used to estimate the relevance of the proposed method, called "1Eq. model" in the following. Sauter mean diameters are measured in a column of 0.4m of diameter with a dual-probe cross-correlation method. Demineralized water is used for experiments, and an air flow rate corresponding to a V_{sg} from 3 to 35cm/s is used. Details are available in the cited article. In order to compute the model, the dissipation rate is required. A first possibility is to use the results of CFD simulations to estimate ε. Here the simulations results of Gemello et al. (2019) are used. 3D simulations were performed with the Euler-Euler model of Ansys Fluent 18.0. The RNG k-ε turbulence model was used. A 40,000 cells mesh was selected after a mesh-dependency study. More details are furnished in the cited paper, but one important information to know is that no specific source terms associated to the presence of bubbles (so called Bubble Induced Turbulence) were introduced in k and ε equations. However, as pointed out by authors the results are sensitive to the turbulence modelling, and can lead to important differences on ε. To overcome this issue, another solution consists to use a theoretical estimation of ε in bubble columns. The theoretical value of ε is calculated by a simple energy balance on the potential energy of gas: $\varepsilon = g.V_{sg}$, though other authors suggest alternative theoretical formulations

(Roels & Heijnen, 1980). Both possibilities, CFD and theoretical calculations, are explored to estimate ε.

Experimental data of Cappello et al. (2020) are used to investigate the case of stirred reactors. The same bubble size measurement method were used as before, with the same water quality, which makes common data processing very consistent. Average bubble sizes are measured in a standard stirred tank of 0.3m of diameter, equipped with a Rushton turbine. The average dissipation rate is estimated from the Power number, measured as 5.5, and using the model of Gabelle et al. (2011) to estimate the loss of power induced by the presence of gas phase (also called Relative Power Demand). Table 3 reports a summary of experimental data used in the present study.

Table 3: Experimental Data

Bubble column (Gemello et al. 2018)

V_{sg} (m/s)	Theoretical ε (m^2/s^3)	CFD ε (m^2/s^3)	α (−)	d_{32} exp. (m)
0.03	0.29	0.07	0.11	0.0075
0.06	0.59	0.13	0.16	0.0076
0.09	0.88	0.26	0.19	0.0072
0.16	1.57	0.56	0.25	0.0078
0.25	2.45	0.95	0.29	0.0085
0.35	3.43	1.38	0.33	0.0085

Stirred reactor (Cappello et al. 2020)

V_{sg} (m/s)	N (rpm)	ε (m^2/s^3)	α (−)	d_{32} exp. (m)
0.0042	600	1.26	0.04	0.0036
0.0042	700	1.99	0.06	0.0034
0.0042	800	2.98	0.08	0.0035
0.0042	900	4.24	0.09	0.0034
0.0042	997	5.76	0.09	0.0035
0.0083	600	0.93	0.05	0.0038
0.0083	700	1.48	0.07	0.0038
0.0083	800	2.20	0.08	0.0036
0.0083	900	3.14	0.10	0.0038
0.0083	997	4.26	0.11	0.0037
0.0208	600	0.73	0.08	0.0045
0.0208	700	1.15	0.10	0.0044
0.0208	800	1.72	0.11	0.0042
0.0208	900	2.45	0.13	0.0042
0.0208	997	3.33	0.14	0.0042
0.0415	600	0.73	0.13	0.0048
0.0415	700	1.15	0.15	0.0048
0.0415	800	1.72	0.17	0.0046
0.0415	900	2.45	0.18	0.0046
0.0415	997	3.33	0.19	0.0046

Raimundo et al. (2016) estimated the global uncertainty of the cross-correlation method in the range of 10 to 15%, by comparison with other methods. Furthermore, Cappello et al. (2020) made some reproducibility tests on the cross-correlation method and found a standard deviation of 3%. In the present study a global error of +/-10% is considered.

Results

Results are organized in 3 parts. First the 1Eq. model is compared with full QMOM simulations. Then the 1Eq. model is used to compare possible combinations of PBM models separately in a bubble column and a stirred tank. Finally the use of a common set of models is considered to predict bubble size simultaneously for both considered flows.

1Eq. model compared to QMOM

QMOM simulations are based on a 0D 1st order explicit method with a time step of 0.01s. A physical time of 15s is considered to insure the convergence of moments, which is generally achieved after 3 to 5s of simulated time. The initialization of the 6 moments is based on a lognormal distribution, based on d_{32}=0.008m and a variance of 0.04. The Wheeler algorithm (Marchisio & Fox, 2013) is used to calculate the weights w_i and abscissa L_i of the quadrature approximation from the m_0 to m_5 moments. The 1Eq. model uses an initial Sauter mean diameter of 8mm. An explicit first order method is used to solve Eq.4 during 15s to achieve stable result, with a time step of 0.01s. Alternatively an iterative method can be used to solve Eq.5, leading to exactly the same results. The comparison between d_{32} models is done with the following kernel: breakage model of Laakkonen (bLa), coalescence frequency of Wang (cfW), coalescence efficiency of Lehr (ceLe), and the daughter size distribution of Laakkonen. No

correction factor (cf) is applied here. 28 arbitrary flow conditions are used for this comparison: α = 5%, 10%, 20% and 40% and ε = 0.1, 0.2, 0.4, 0.8, 1.6, 3.2, 6.4 m^2/s^3.

The parity diagram between both models results is reported on Figure 1. The average error of the 1Eq. model compared with QMOM is 2.9%, which represents approximately 0.2mm for a bubble diameter of 8mm. Therefore, this difference is considered to be sufficiently low to validate the use of the 1Eq. model to compare kernels.

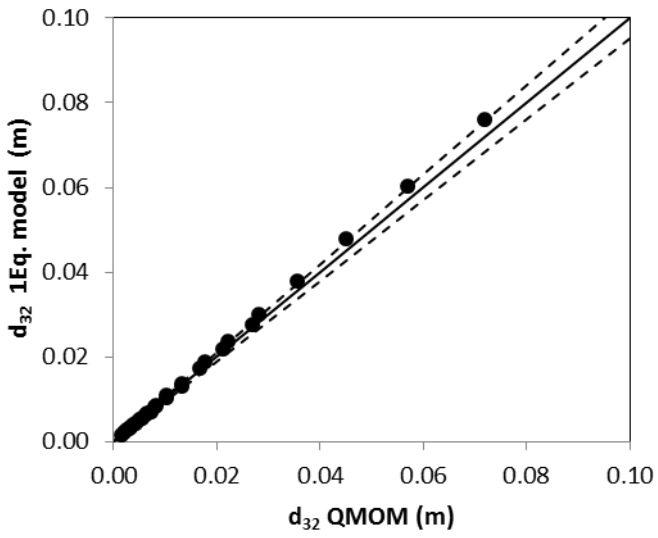

Figure 1: Parity diagram of the 1Eq. model Versus the QMOM model.

Different benefits are associated with the use of the 1Eq. model. First, the calculation time associated to this method is lower than with the QMOM, as no reconstruction algorithm is used. The 1Eq. model is approximately 80 times faster than the QMOM with the Wheeler reconstruction algorithm. This could make a difference in case of multi-variable optimization. The simplicity of the 1Eq. model is also advantageous in case of implementation in a CFD code. Secondly, for a given set of PBM kernels, the estimation of the correction factor *cf* that optimizes predictions is fast and simple as discussed above. And at last, the effect of breakage and coalescence kernels on d_{32} is explicitly described: the Eq.5 can be recombined as the

dimensionless ratio between the breakage frequency $g(L)$ and the coalescence frequency $6\alpha.h_0(L,L)\cdot\lambda(L,L)/(\pi.L^3)$, both in s^{-1}:

$$\frac{6\alpha.h(L,L)/(\pi.L^3)}{g(L)} = \left(\bar{b}^2/L^2 - 1\right)/\left(1 - 2^{-\frac{1}{3}}\right) \quad (7)$$

The left hand term is the ratio between coalescence and breakage frequencies. The right hand term is a function of the daughter size distribution and its effect on the interfacial area. Left term of Eq.7, is likewise the ratio between characteristic times of breakage and coalescence τ_b/τ_c. Finally, by multiplying Eq.4 by π, the stable bubble size is the one that equalizes the rate of increase of interfacial area due to breakage $\frac{6\alpha}{L}g(L)(b^2/L^2-1)$ with the rate of interfacial area loss due to coalescence $\frac{18\alpha^2}{\pi L^4}h(L,L)\left(2-2^{\frac{2}{3}}\right)$ in $m^2.m^{-3}.s^{-1}$. The 1Eq. model is used to compare the 60 possible combinations of models reported in Table 1. As discussed in the last section, the choice of the daughter size distribution model β changes the fit of the correction factor *cf*, but not the calculations of d_{32}. Therefore, all calculations are performed with the daughter size distribution model of Laakkonen.

However, it is very important to notice that the 1Eq. model does not replace the full QMOM. As only the m_2 transport equation is solved, the estimation of other moments of the BSD, possible from α and d_{32}, is subject to caution. No information about the BSD is predicted apart the Sauter mean diameter. For this reason, the 1Eq. model can be considered for many applications as a preliminary shortcut before using a QMOM or multiclass method.

For each combination of models, the correction factor *cf* is computed in order to optimize the fit with the considered dataset. The fit process is as follows. a)*cf* is equal to 1 initially. b) the Sauter mean diameter is computed for each condition of the dataset. c) *cf* is replaced by the ratio $cf \times \overline{d_{32,exp}}/\overline{d_{32,calc}}$ and the step b) is repeated. $\overline{d_{32,exp}}$ is the average Sauter diameter over the experimental dataset, and $\overline{d_{32,calc}}$ is the average of the calculated Sauter diameters over the same dataset. the Sauter mean diameters are updated until *cf* is stable, with an evolution lower

than 10^{-5} between two iterations. A ratio $\overline{d_{32,exp}}/\overline{d_{32,calc}} < 1$ indicates that too big bubbles are predicted in average and that a lower value of *cf* may lead to more realistic results.

For Bubble columns, the fit is done while considering consecutively the dissipation rate estimated by CFD, or by the theoretical approach as discussed earlier. For each case, the 10 best fits are reported in Table 4. In agreement with the experimental uncertainty, the ranking between models that exhibits less than 10% of the root mean square error is subject to caution.

Table 4: Results of the parameter fit (best 10 combinations for each dataset)

Bubble Column ε from CFD			**Bubble Column Theoretical ε**			**Stirred Reactor**		
Model	Error	*cf*	Model	Error	*cf*	Model	Error	*cf*
bLa,cfW,ceLe	4.3%	1.00E+00	bLa,cfPB,ceLe	4.5%	4.95E-01	bCT,cfPB,ceLe	6.8%	1.43E-04
bLa,cfLe,ceLe	6.9%	1.74E+00	bLa,cfPB,ceC	6.8%	2.96E-01	bCT,cfW,ceLe	7.4%	5.64E-04
bLa,cfPB,ceC	7.0%	1.96E-01	bLa,cfW,ceC	7.8%	9.77E-01	bCT,cfPB,ceC	7.8%	5.68E-05
bLa,cfW,ceC	8.4%	6.42E-01	bLa,cfLe,ceC	10.1%	1.68E+00	bCT,cfW,ceC	8.5%	2.33E-04
bLa,cfPB,ceLe	9.0%	3.15E-01	bPB,cfPB,ceC	11.4%	8.26E-03	bCT,cfC,ceLe	9.0%	3.92E-02
bLa,cfLe,ceC	10.7%	1.10E+00	bLa,cfW,ceLe	11.8%	1.58E+00	bCT,cfLe,ceLe	9.2%	1.09E-03
bPB,cfPB,ceC	13.1%	5.53E-03	bCT,cfPB,ceLe	14.0%	3.26E-04	bCT,cfLe,ceC	9.9%	4.54E-04
bCT,cfPB,ceLe	14.1%	3.26E-04	bCT,cfPB,ceC	14.2%	1.70E-04	bCT,cfC,ceC	10.1%	1.60E-02
bCT,cfPB,ceC	19.3%	1.86E-04	bLa,cfLe,ceLe	14.3%	2.70E+00	bLa,cfLe,ceCT	13.5%	3.11E+09
bLa,cfC,ceC	19.4%	4.34E+01	bLa,cfC,ceC	14.5%	5.49E+01	bLa,cfPB,ceCT	13.6%	4.39E+08

Case of a bubble column

Concerning the investigated bubble column, the best results are obtained with the following kernel: Laakkonen model for breakage, Wang or Prince & Blanch models for collision frequency, and Lehr or Chesters models for coalescence efficiency. These conclusions meet the ones of Gemello et al. (2019) using CFD and QMOM. Gemello et al. (2019) found that coalescence efficiency models based on film drainage theory are not appropriate due to the fall of the coalescence rate with V_{sg}, and pointed out the relevance of the association of the Laakkonen model (breakage) with the Wang model (coalescence frequency) and Lehr model (coalescence efficiency). The latter combination is also found as the most appropriate in the present study,

which reinforces previous conclusions of Gemello et al., as a wider screening of models is performed here. The Figure 2 illustrates the error associated with the combinations when errors are below 180%. 5 combinations exhibit an error below the experimental uncertainty of 10%. Figure 3 reports results on bubble columns for both ε calculations. All reported combinations stand within the experimental error bar, excepted at low V_{sg}.

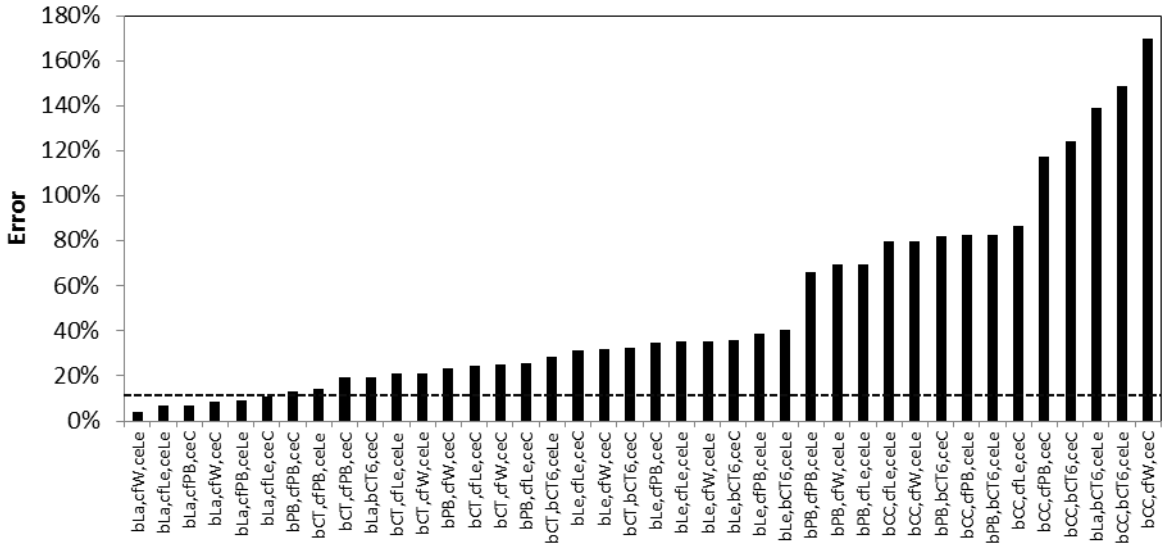

Figure 2: Error associated to 40 kernel combinations (case of bubble columns).

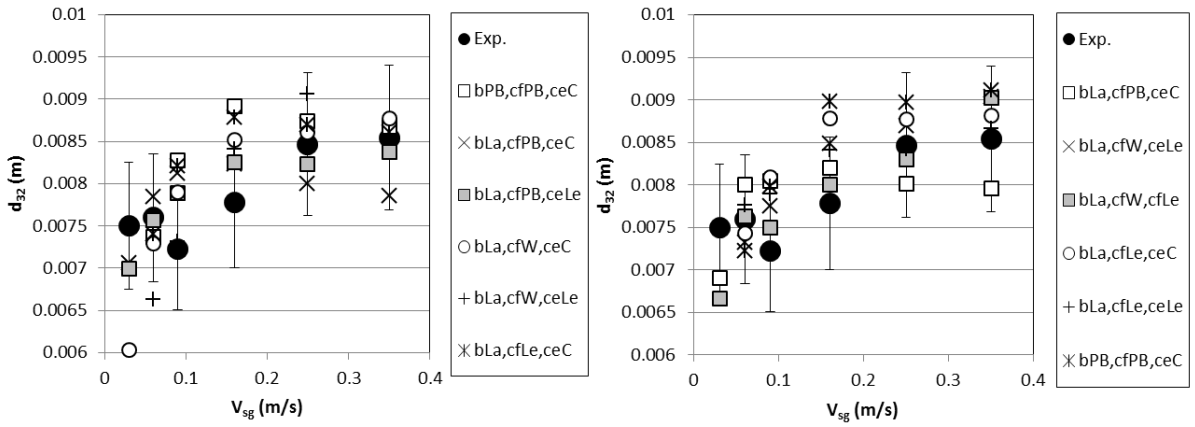

Figure 3: Comparison of d_{32} between experiments and best PBM combinations in the bubble column, as functions of V_{sg}. Left: ε computed from CFD simulations of Gemello et al. (2019), right: Theoretical calculation of ε. The error bars of +/- 10% are reported on experimental data.

Case of a stirred reactor

The same procedure of *cf* computing, as described above for the bubble column, is now carried out for an aerated stirred tank, with the dataset of Cappello et al. (2020). Figure 4 reports, in the case of stirred tanks, the errors associated to the 33 best kernel combinations. Unshowned combinations lead to errors >200%. The first combinations exhibit very similar deviations from experiments (comprises between 6.8% to 9.2%), all being within the experimental uncertainty. The classical breakage model of Coulaloglou & Tavlarides is confirmed as relevant, but a significant constant adjustment has to be done (*cf* deviates strongly from 1). Concerning coalescence, the same models than for bubble columns are found as relevant. Prince & Blanch and Wang models concerning coalescence frequency, and Lehr and Chesters models concerning coalescence efficiency. The four best model combinations are reported on Figure 5 and compared to experimental results at stirring rates of 700 and 900 RPM, respectively.

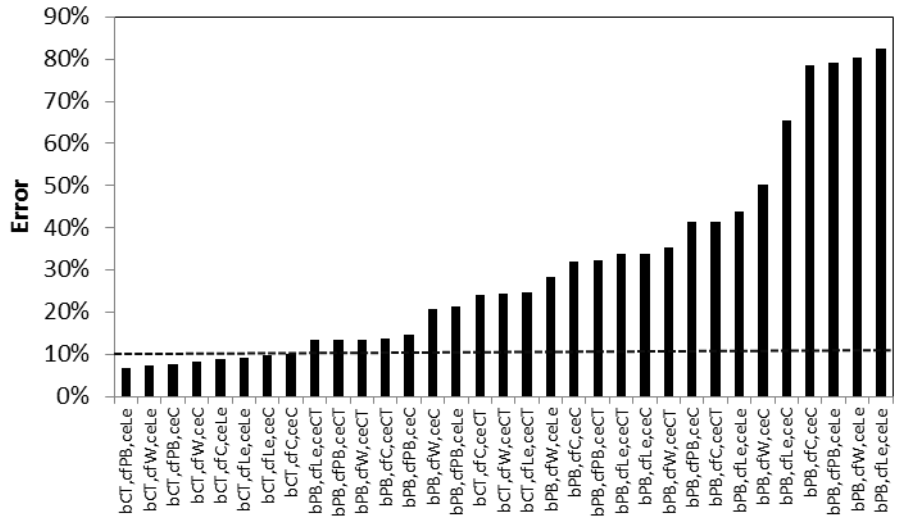

Figure 4: Error associated to 33 kernel combinations (case of a stirred tank).

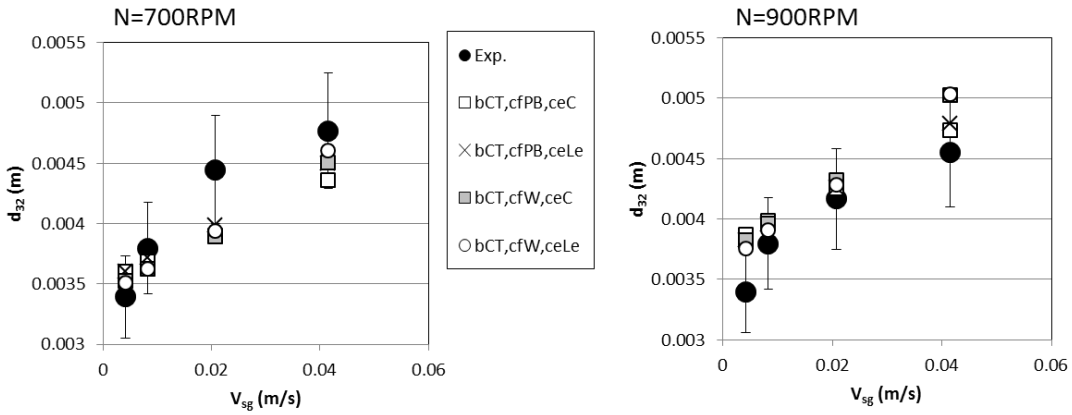

Figure 5: Comparison of d_{32} between experiments and best PBM combinations in a stirred tank, as functions of V_{sg}. Left: stirring rate of 700 RPM, right: stirring rate of 900 RPM. Same symbols on both graphs. The error bars of +/- 10% are reported on experimental data.

A conclusion concerning model selection, when operated separately on a bubble column and a stirred reactor, is that two different breakage models are selected: the model of Laakkonen for the bubble column, and the model of Coulaloglou & Tavlarides for the stirred reactor.

Finally, while using the 1Eq. model, there is no need to associate *cf* to a modification of breakage or coalescence kernel as both phenomena are assumed in equilibrium. But further use in CFD or transient simulations may require to associate the parameter fit to a specific model. Gemello et al. (2019) fitted the first constant of the collision frequency model and obtained satisfying results, even in the part of the column where bubble size is governed by the breakage rate. For this reason, if necessary, it is preferred to associate the fit of the *cf* coefficient to the first constant of the collision frequency model.

Combined cases

Best kernels for each flow configuration are different, so finally a parameter fit was processed in order to investigate the possibility of identifying a kernel adapted to both experimental data

simultaneously. Two combinations of models appear relevant: bLa, cfPB, ceC (mean error of 16.9%, *cf*=0.26), and bLa, cfW, ceLe (mean error of 17.9%, *cf*=2.37). The best fit is reported on the parity diagram in Figure 6. Mean errors are higher than the experimental error (10%), and 2.5 to 3 times higher than those associated to a separated fit on each flow configuration. Although the results cannot be generalized to any bubbly flows, these 2 models combinations appear as able to cover various hydrodynamic regimes, and can thus be considered as relatively robust. Internal parameters of kernels has not been adjusted to optimize results, and it cannot be excluded that that such an additional parameter fit could improve results.

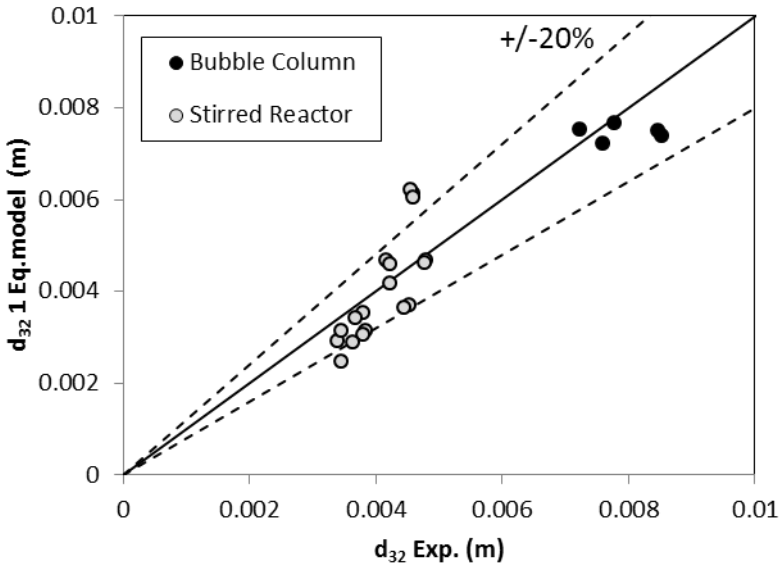

Figure 6: Parity diagram of the global dataset (bubble column + stirred tank), with the breakage model of Laakkonen, collision frequency model of Prince & Blanch and coalescence efficiency of Chesters (cf=0.26*).*

Conclusion

On the basis of QMOM theoretical background, a simple model has been developed to predict stable Sauter mean diameters in bubbly flows. The model can be used to quickly optimize any

set of population balance models, and to screen optimized kernels in any set of experimental conditions. The model delivers Sauter mean diameter very close to the ones obtained with the more rigorous QMOM method (less than 3% of difference), but it does not provide for any other characteristic of the bubble size distribution. It has been applied to identify, among 60 possible combinations, the better kernel combinations for two types of reactors operated under various flow conditions: a bubble column and an aerated stirred tank. Besides two different kernel combinations have been found to deliver rather good predictions simultaneously on both considered cases. The collision frequency modes of Prince & Blanch (1990) and its variant developed by Wang et al. (2005) are found as relevant for both flows. The coalescence efficiency models of Lehr & Mewes (1999) and Chesters (1991) are also found as the best choices to fit the experimental data used in this study. Concerning breakage frequency, the model of Laakkonen et al. (2006) gives the best results for the bubble column, while the model of Coulaloglou & Tavlarides (1977) is preferred for the data concerning the stirred tank. Results obtained on the bubble column, with the 1Eq. model, confirm those obtained previously by Gemello et al. (2019), based on the coupling of QMOM with 3D CFD simulations. A first perspective of the 1Eq. model concerns its implementation in CFD codes to simulate stirred reactors and bubble columns, and to compare results with CFD/QMOM simulations. Another perspective would be to investigate of the effect physical properties (rheology, interfacial properties) on bubble sizes, and the way to implement them on population balance models.

Nomenclature

Notation

$\bar{b}_i^k$	k^{th} moment of β, m^k
cf	correction factor, -
d_{32}	Sauter mean diameter, m
$\overline{d_{32,exp}}$	average experimental Sauter mean diameter, m
$\overline{d_{32,calc}}$	average calculated Sauter mean diameter, m
g	gravity acceleration, m s^{-2}
g	breakage kernel, s^{-1}
h_0	collision frequency, m^3 s^{-1}
k	order of moment
L_i	node of the quadrature approximation, m
m_k	moment of order k of the BSD, m^{k-3}
N_q	order of the quadrature approximation -
u_{crit}	critical velocity, $m.s^{-1}$
V_{sg}	superficial gas velocity, $m.s^{-1}$
w_i	weights of the quadrature approximation, m^{-3}

Greek symbols

α	gas volume fraction, -
β	daughter distribution function, -
α_{max}	maximal value of gas volume fraction, -
ε	turbulence dissipation rate, m^2 s^{-3}
λ	coalescence efficiency, -
ν	kinematic viscosity of the liquid phase, m^2 s^{-1}
ρ_G	density of the gas phase, $kg.m^{-3}$

ρ_L density of the liquid phase, kg.m^{-3}

σ surface tension, N.m^{-1}

τ_b characteristic breakage time, s

τ_c characteristic coalescence time, s

References

Buffo, A., Vanni, M., Marchisio, D.L., Fox, R.O., 2013. Multivariate Quadrature-Based Moments Methods for turbulent polydisperse gas-liquid systems. Int. J. Multiph. Flow. 50, 41–57.

Cappello, V., Plais, C., Vial, C., Augier, F., 2020. Bubble size and liquid-side mass transfer coefficient measurements in aerated stirred tank reactors with non-Newtonian liquids. Chem. Eng.Sci, 211,https://doi.org/10.1016/j.ces.2019.115280.

Carrica, P. M. & Clausse, A. A., 1993. A Mathematical Description of the Critical Heat Flux as Nonlinear Dynamic Instability, G. Gouesbet and A. Berlemont.Instabilities in Multiphase Flow, Plenum Press, New York.

Chesters, A. K.,1991, The modeling of coalescence processes in fluid-liquid dispersions:A review of current understanding, Chemical Engineering Research and Design: transactions of the Institution of Chemical Engineers: Part A69, 259–270.

Coulaloglou, C. A. & Tavlarides, L. L., 1977.Description of interaction processesin agitated liquid-liquid dispersions. Chem. Eng. Sci. 32, 1289–1297.

Gabelle, J.C., Augier, F., Carvalho, A., Rousset, E., Morchain, J., 2011. Effect of Tank Size on kLa and Mixing Time in Aerated Stirred Reactors With Non-Newtonian Fluids. Can.J.Chem.Eng. 89, 1139-1153.

Garcia-Ochoa, F. Gomez, E., 2009. Bioreactor scale-up and oxygen transfer rate in microbial processes: An overview. Biotech. Adv. 27, 153-176.

Gemello, L., 2018, Modelling of the hydrodynamics of bubble columns using a two-fluid model coupled with a population balance approach. PhD Thesis of the University of Lyon.

Gemello, L., Plais, C., Augier, F., Cloupet, A., Marchisio, D.L., 2018. Hydrodynamics and bubble size in bubble columns: Effects of contaminants and spargers, Chem. Eng. Sci. 184, 93-102.

Gemello, L., Plais, C., Augier, F., Marchisio, D.L., 2019. Population balance modelling of bubble columns under the heterogeneous flow regime. Chem. Eng. J., 372, 590-604.

Laakkonen, M., Alopaeus, V., Aittamaa, J., 2006. Validation of bubble breakage,coalescence and mass transfer models for gas-liquid dispersion in agitated vessel. Chem. Eng. Sci. 61, 218–228.

Lane, G.L., Schwarz, M.P., Evans, G.M., 2005. Numerical modelling of gas–liquid flow in stirred tanks. Chem. Eng. Sci., 60, 2203 – 2214.

Lasheras, J. C., Eastwood, C., Martínez-Bazán, C. & Montañés, J. L., 2002. Areview of statistical models for the break-up of an immiscible fluid immersedinto a fully developed turbulent flow. Int. J. of Mult. Flow, 28, 247–278.

Lehr, F. & Mewes, D. 1999. A transport equation for the interfacial area density applied to bubble columns. Chem. Eng. Sci., 56, 1159–1166.

Liao, Y., Lucas, D., 2009. A literature review of theoretical models for drop and bubble breakup in turbulent dispersions. Chem. Eng. Sci., 64, 3389–3406.

Liao, Y., Lucas, D., 2010. A literature review on mechanisms and models for the coalescence process of fluid particles, Chem. Eng. Sci. 65, 2851–2864.

McGraw, R., 1997. Description of Aerosol Dynamics by the Quadrature Method of Moments. Aerosol Sci. Tech. 27, 255-265.

Marchisio, D.L., Pikturna, J.T., Fox, R.O., Vigil, R.D., Barresi A.A., 2003. Quadrature Method of Moments for Population-Balance Equations. AIChE J., 49, 5, 1266-1276.

Marchisio, D.L., Fox, R.O., 2013. Computational Models for Polydisperse Particulate and Multiphase Systems, Cambridge Series in Chemical Engineering, Cambridge University Press, Cambridge, UK.

Raimundo M.P., Cartellier A., Beneventi D., Forret A., Augier F., 2016. A new technique for in-situ measurements of bubble characteristics in bubble columns operated in the heterogeneous regime, Chem. Eng. Sci., 155 , 504-523.

Petitti, M., Nasuti, A., Marchisio, D.L., Vanni, M., Baldi, G., Mancini, N.,Podenzani F., 1990. Bubble size distribution modeling in stirred gas-liquid reactors with QMOM augmented by a new correction algorithm, Am. Inst. Chem. Eng. J., 56, 36–53.

Prince, M. J. & Blanch, H. W., 1990. Bubble coalescence and break-up in air sparged bubble columns. AIChE J., 36, 1485–1499.

Roels, J.A., Heijnen J.J, 1980. Power dissipation and heat production in bubble columns: approach based on nonequilibrium thermodynamics.Biotechnol. Bioeng., 22,11, 2399–2404.

Wang, T.F., Wang, J.F.W, Jin, Y., 2005. Population balance model for gas-liquid flows: Influence of bubble coalescence and breakup models. Ind. Eng. Chem. Res. 44,11, 7540–7549.

Tables captions

Table 1: Population balance models used in the study. B: breakage, CF: collision frequency, CE: coalescence efficiency

Table 2: Considered Models of binary daughter size distribution

Table 3: Experimental Data

Table 4: Results of the parameter fit (best 10 combinations for each dataset)

Figures captions

Figure 1: Parity diagram of the 1Eq. model Versus the QMOM model.

Figure 2: Error associated to 40 kernel combinations (case of bubble columns).

Figure 3: Comparison of d_{32} between experiments and best PBM combinations in bubble columns, as functions of V_{sg}. Left: ε computed from CFD simulations of Gemello et al. (2019), right: Theoretical calculation of ε. The error bars of +/- 10% are reported on experimental data.

Figure 4: Error associated to 33 kernel combinations (case of stirred tanks).

Figure 5: Comparison of d_{32} between experiments and best PBM combinations in a stirred tank, as functions of V_{sg}. Left: Stirring rate of 700 RPM, right: Stirring rate of 900 RPM. Same symbols on both graphs. The error bars of +/- 10% are reported on experimental data.

Figure 6: Parity diagram of the global dataset (bubble column+stirred tank), with the Breakage model of Laakkonen, Collision frequency model of Prince & Blanch and coalescence efficiency of Chesters (cf=0.26*).*